MUMT 618: Week #9

1 Tonehole Modeling

Woodwind toneholes not only provide a means for bore length variation but also control sound radiation behavior according to their radius, height, and if present, keypad location. The influence of open and closed toneholes on wave propagation within a musical instrument bore greatly complicates the ideal behaviors previously discussed.

1.1 A Two-Port Tonehole Model

- The fundamental acoustic properties of toneholes have been extensively studied and reported by Keefe [1981, 1990a], Dubos et al. [1999], Dalmont et al. [2002], Nederveen et al. [1998], Lefebvre and Scavone [2012].
- The model described by Keefe [1990a] is an accurate representation for a tonehole unit, assuming adjacent tonehole interactions are negligible.
- In this description, acoustic variables at the tonehole junction are related by a transfer matrix of series and shunt impedance parameters.
- Keefe's original derivation of the tonehole parameters was based on a symmetric T section, as shown in Fig. 1 [Keefe, 1981].

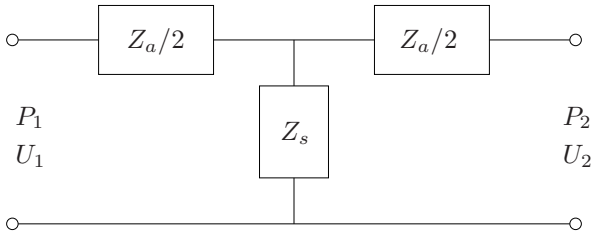

Figure 1: T section transmission-line representation of the tonehole.

- The series impedance terms, Z_a, result from an analysis of anti-symmetric pressure distribution, or a pressure node, at the tonehole junction. In this case, volume flow is symmetric and equal across the junction.
- The shunt impedance term, Z_s, results from an analysis of symmetric pressure distribution, or a pressure anti-node, at the tonehole, for which pressure is symmetric and equal across the junction.
- The transfer matrix that results under this analysis is given by

$$\begin{aligned} \begin{bmatrix} P_1 \\ U_1 \end{bmatrix} &= \begin{bmatrix} 1 & Z_a/2 \\ 0 & 1 \end{bmatrix} \begin{bmatrix} 1 & 0 \\ Z_s^{-1} & 1 \end{bmatrix} \begin{bmatrix} 1 & Z_a/2 \\ 0 & 1 \end{bmatrix} \begin{bmatrix} P_2 \\ U_2 \end{bmatrix} \\ &= \begin{bmatrix} 1+\frac{Z_a}{2Z_s} & Z_a\left(1+\frac{Z_a}{4Z_s}\right) \\ Z_s^{-1} & 1+\frac{Z_a}{2Z_s} \end{bmatrix} \begin{bmatrix} P_2 \\ U_2 \end{bmatrix}. \end{aligned} \tag{1}$$

obtained by cascading the three matrices that correspond to the three impedance terms.

- Based on the approximation that $|Z_a/Z_s| \ll 1$, Eq. (1) can be reduced to the form

$$\begin{bmatrix} P_1 \\ U_1 \end{bmatrix} = \begin{bmatrix} 1 & Z_a \\ Z_s^{-1} & 1 \end{bmatrix} \begin{bmatrix} P_2 \\ U_2 \end{bmatrix}, \tag{2}$$

  which is the basic tonehole unit cell given by Keefe for transfer-matrix calculations.

- The values of Z_a and Z_s vary according to whether the tonehole is open (o) or closed (c) as

$$\begin{aligned} Z_s^{(o)} &= Z_c(a/b)^2 \, (jkt_e + \xi_e), & (3)\\ Z_s^{(c)} &= -jZ_c(a/b)^2 \cot(kt), & (4)\\ Z_a^{(o)} &= -jZ_c(a/b)^2 kt_a^{(o)}, & (5)\\ Z_a^{(c)} &= -jZ_c(a/b)^2 kt_a^{(c)}. & (6) \end{aligned}$$

- Definitions and descriptions of the various parameters in Eqs. (3) – (6) can be found in [Keefe, 1990a].

- To render these relationships in the digital waveguide domain, it is necessary to transform the plane-wave physical variables of pressure and volume velocity to traveling-wave variables as

$$\begin{bmatrix} P_1 \\ U_1 \end{bmatrix} = \begin{bmatrix} P_1^+ + P_1^- \\ Z_c^{-1}\left(P_1^+ - P_1^-\right) \end{bmatrix}, \tag{7}$$

  where Z_c is the characteristic impedance of the cylindrical bore, which is equal on both sides of the tonehole.

- Waveguide pressure variables on both sides of the tonehole are then related by

$$\begin{bmatrix} P_1^- \\ P_2^+ \end{bmatrix} = \begin{bmatrix} \mathcal{R}^- & \mathcal{T}^- \\ \mathcal{T}^+ & \mathcal{R}^+ \end{bmatrix} \begin{bmatrix} P_1^+ \\ P_2^- \end{bmatrix}, \tag{8}$$

  where

$$\begin{aligned} \mathcal{R}^- = \mathcal{R}^+ &\approx \frac{Z_a Z_s - Z_c^2}{Z_a Z_s + 2Z_c Z_s + Z_c^2}, & (9)\\ \mathcal{T}^- = \mathcal{T}^+ &\approx \frac{2Z_c Z_s}{Z_a Z_s + 2Z_c Z_s + Z_c^2}, & (10) \end{aligned}$$

  calculated using Eqs. (1) and (7) and then making appropriate simplifications for $|Z_a/Z_s| \ll 1$.

- Figure 2 depicts the waveguide tonehole two-port scattering junction in terms of these reflectances and transmittances. This structure is analogous to the four-multiply Kelly-Lochbaum scattering junction [Kelly and Lochbaum, 1962].

- For the implementation of the reflectances and transmittances given by Eqs. (9) – (10) in the digital waveguide structure of Fig. 2, it is necessary to convert the continuous-time filter responses to appropriate discrete-time representations.

- Results of this approach are shown in Figure 3 and are compared with reproduced results using the technique of Keefe [Keefe, 1990a] for a simple flute air column with six toneholes.

- The implementation of a sequence of toneholes in this way is diagrammed in Figure 4.

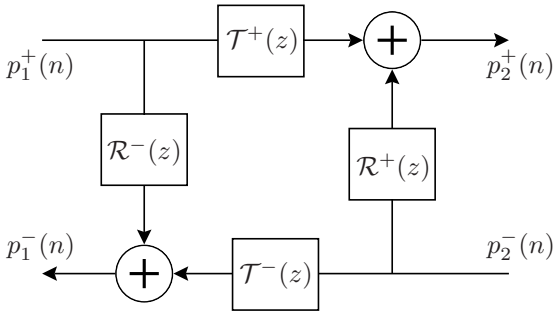

Figure 2: Digital waveguide tonehole two-port scattering junction.

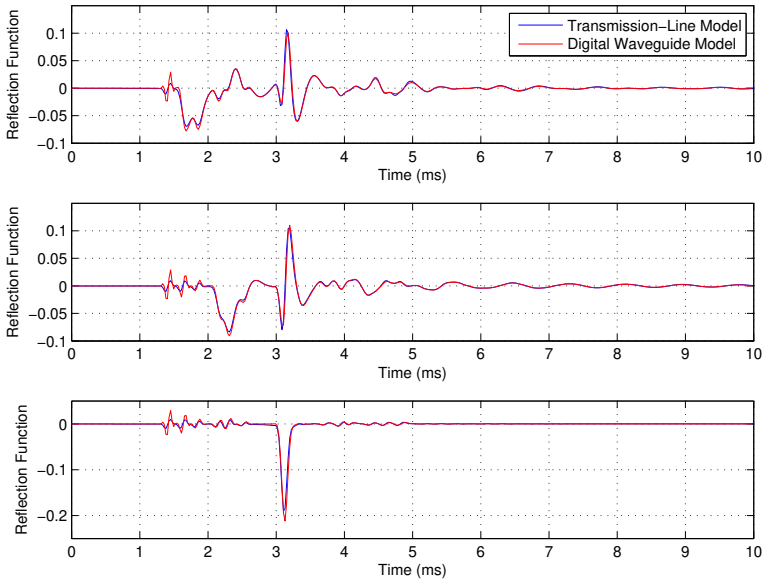

Figure 3: Calculated reflection functions for a simple flute air column [see [Keefe, 1990a]]. Transmission line model vs. DW two-port model with one hole closed (top), three holes closed (middle), and six holes closed (bottom).

1.2 A Three-Port Tonehole Model

- For the purpose of real-time modeling, the two-port implementation has a particular disadvantage: the two lumped characterizations of the tonehole as either closed or open cannot be efficiently unified into a single tonehole model.
- It is preferable to have one model with adjustable parameters to simulate the various states of the tonehole, from closed to open and all states in between.
- To this end, it is best to consider a distributed model of the tonehole, such that "fixed" portions of the tonehole structure are separated from the "variable" component.
- The junction of the tonehole branch with the main air column of the instrument can be modeled in the DW domain using a three-port scattering junction, as described in Scavone [1997].
- This method inherently models only the shunt impedance term of the Keefe tonehole characterization, however, the negative length correction terms implied by the series impedances can be approximated by adjusting the delay line lengths on either side of the three-port scattering junction.

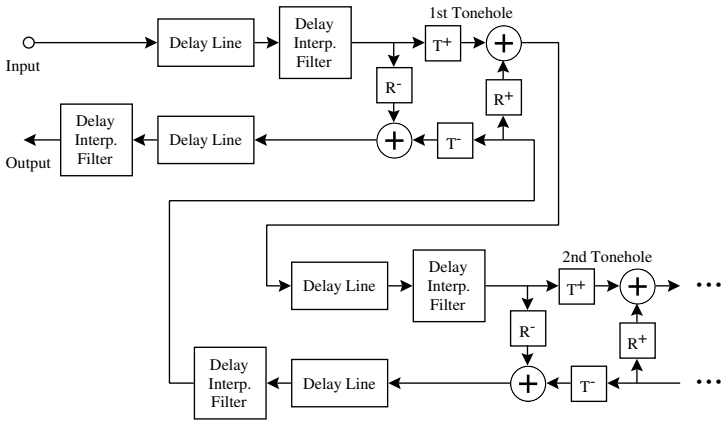

Figure 4: Digital waveguide two-port tonehole implementation scheme, including delay-line length interpolation filters.

- The other "fixed" portion of the tonehole is the short branch segment itself, which is modeled in the DW domain by appropriately sized delay lines.
- This leaves only the characterization of the open/closed tonehole end.
- A simple inertance model of the open hole end offers the most computationally efficient solution. The impedance of the open end is then given by

$$Z_e^{(o)}(s) = \frac{\rho t}{A_e} s, \tag{11}$$

  where ρ is the density of air, A_e is the cross-sectional area of the end hole, t is the effective length of the opening ($\approx A_e^{1/2}$), and s is the Laplace transform frequency variable.

- The open-end reflectance is

$$\mathcal{R}_e^{(o)}(s) \stackrel{\Delta}{=} \frac{P_e^-(s)}{P_e^+(s)} = \frac{Z_e^{(o)}(s) - Z_{cb}}{Z_e^{(o)}(s) + Z_{cb}} = \frac{tA_b s - cA_e}{tA_b s + cA_e}, \tag{12}$$

  where $Z_{cb} = \rho c / A_b$ is the characteristic impedance of the tonehole branch waveguide, A_b is the cross-sectional area of the branch and c is the speed of sound.

- An appropriate discrete-time filter implementation for $\mathcal{R}_e^{(o)}$ can be obtained using the conformal bilinear transform from the s-plane to the z-plane [Oppenheim and Schafer, 1989, pp. 415-430], with the result

$$\mathcal{R}_e^{(o)}(z) = \frac{a - z^{-1}}{1 - az^{-1}}, \tag{13}$$

  where

$$a = \frac{tA_b\alpha - cA_e}{tA_b\alpha + cA_e} \tag{14}$$

  and α is the bilinear transform constant that controls frequency warping.

- The discrete-time reflectance $\mathcal{R}_e^{(o)}(z)$ is a first-order allpass filter, which is consistent with reflection from a "masslike" impedance.
- It is possible to simulate the closing of the tonehole end by taking the end hole radius (or A_e) smoothly to zero.

- In the above implementation, this is accomplished simply by varying the allpass coefficient between its fully open value and a value nearly equal to one.
- With $a \approx 1$, the reflectance phase delay is nearly zero for all frequencies, which corresponds well to pressure reflection at a rigid termination.
- A complete implementation scheme is diagrammed in Figure 5.

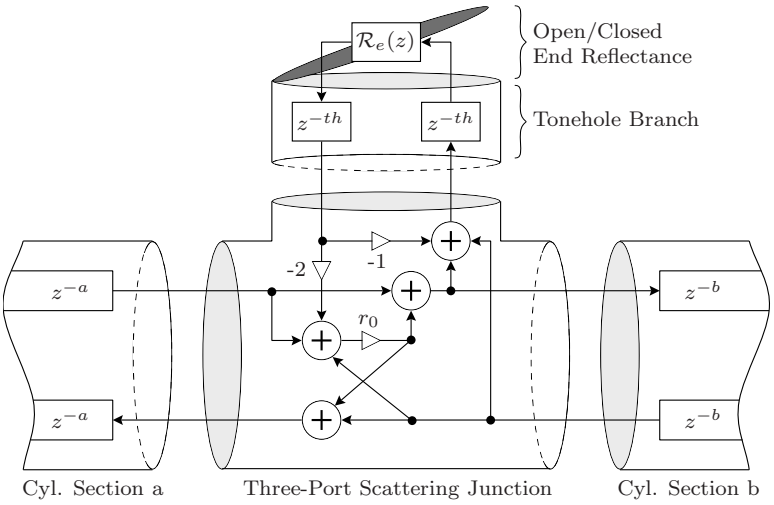

Figure 5: "Distributed" digital waveguide tonehole implementation.

- Figure 6 shows the reflection functions obtained using this model in comparison to the Keefe transmission-line results.
- This efficient model of the tonehole produces results very much in accord with the more rigorous model.
- A more accurate model of the tonehole branch end, which is not pursued here, would include a frequency-dependent resistance term and require the variation of three first-order filter coefficients.

1.3 Register Hole Models

- Woodwind register holes are designed to discourage oscillations based on the fundamental air column mode and thus to indirectly force a vibratory regime based on higher, more stable resonance frequencies.
- A register vent functions both as an acoustic inertance and an acoustic resistance [Benade, 1976]. It is ideally placed about one-third of the distance from the excitation mechanism of a cylindrical-bored instrument to its first open hole.
- Sound radiation from a register hole is negligible.
- The DW implementation of a register hole can proceed in a manner similar to that for the tonehole. The series impedance terms associated with toneholes are insignificant for register holes and can be neglected.
- Modeling the open register hole as an acoustic inertance in series with a constant resistance, its input impedance as seen from the main bore is given by

$$Z_{rh}^{(o)}(s) = \frac{\rho t}{A_{rh}} s + \xi, \tag{15}$$

where ρ is the density of air, t is the effective height, A_{rh} is the cross-sectional area of the hole, ξ is the acoustic resistance, and s is the Laplace transform frequency variable.

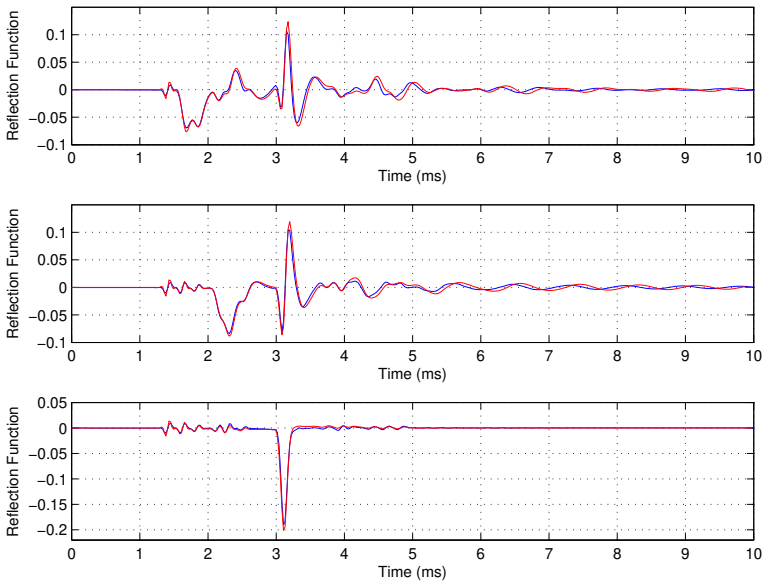

Figure 6: Calculated reflection functions for a simple flute air column [see [Keefe, 1990a]]. Transmissionf line model vs. DW "distributed" tonehole model with one hole closed (top), three holes closed (middle), and six holes closed (bottom).

- Proceeding with a two-port DW implementation, the register hole is represented in matrix form by

$$\begin{aligned}\begin{bmatrix} P_1^- \\ P_2^+ \end{bmatrix} &= \begin{bmatrix} \mathcal{R}^- & \mathcal{T}^- \\ \mathcal{T}^+ & \mathcal{R}^+ \end{bmatrix} \begin{bmatrix} P_1^+ \\ P_2^- \end{bmatrix} \\ &= \frac{1}{Z_c + 2Z_{rh}} \begin{bmatrix} -Z_c & 2Z_{rh} \\ 2Z_{rh} & -Z_c \end{bmatrix} \begin{bmatrix} P_1^+ \\ P_2^- \end{bmatrix}, \end{aligned} \tag{16}$$

  where the open register hole shunt impedance is given by $Z_{rh}^{(o)}$ and Z_c is the characteristic impedance of the main air column.

- The reflectances and transmittances are equivalent at this junction for wave components traveling to the right or to the left. As $\mathcal{T} = 1 + \mathcal{R}$, a one-filter form of the junction is possible.

- Using the bilinear transform, an appropriate discrete-time implementation for $\mathcal{R}_{rh}$ is given by

$$\mathcal{R}_{rh}^-(z) = \mathcal{R}_{rh}^+(z) = \frac{-c\left(1 + z^{-1}\right)}{(\zeta + \alpha\psi) + (\zeta - \alpha\psi)\, z^{-1}}, \tag{17}$$

  where

$$\zeta = c + 2A_0\xi/\rho \qquad \text{and} \qquad \psi = 2A_0 t/A_{rh}, \tag{18}$$

  A_0 is the cross-sectional area of the main air column, and α is the bilinear transform constant that controls frequency warping.

- Assuming the closed register hole has neglible effect in the acoustic model, simulated closure of the register hole in this implementation is achieved by ramping the reflectance filter gain to zero.

- This implementation is similar to that of Välimäki et al. [1993], though resistance effects were not accounted for in that study.

- As discussed by Benade [Benade, 1976, p. 459], a misplaced register hole will raise the frequency of the second air column mode by an amount proportional to its displacement from the ideal location (in either direction).

- Such behavior is well demonstrated when this register hole implementation is added to the real-time clarinet model.

2 Reed Valve Modeling

Wind instruments are "driven" by either pressure- or velocity-controlled valves. In this section we focus on the modeling of pressure-controlled valves, such as the clarinet reed and the brass player's lips. While most of the focus here is on the reed valve, much of the analysis can be equally applied to the lip mechanism as well.

2.1 Pressure-Controlled Reeds

- The single-reed and mouthpiece arrangement of clarinets and saxophones (Fig. 7) acts as a pressure-controlled valve that allows energy into the instrument for the initialization and maintenance of oscillations in the downstream air column.

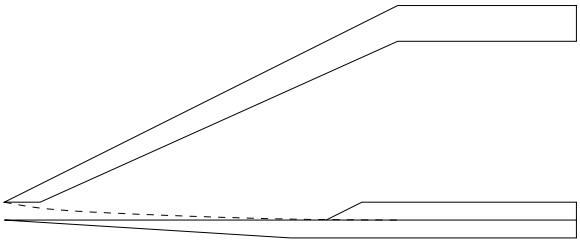

Figure 7: A single-reed woodwind mouthpiece.

- The inherent non-linear behavior of this mechanism, which is attributable to such aspects as the flow characteristic through the reed aperture and the reed's displacement when it hits the mouthpiece facing, is most obviously demonstrated by the fact that a nearly static pressure applied at the upstream side of the system is converted into acoustic energy on the downstream side at a number of harmonically related frequencies.
- The flow and reed movement are controlled by the difference in pressures on the upstream and downstream sides of the reed channel, $p_\Delta = p_u - p_d$.
- The upstream pressure is typically assumed constant or slowly varying and tends to force the reed toward the mouthpiece lay.
- Negative pressure in the mouthpiece reinforces this action, pulling the reed toward the lay, while positive pressure in the mouthpiece, if acting alone, pushes the reed away from the mouthpiece lay.
- The single-reed valve is initially open but can be blown shut against the mouthpiece lay by an appropriate pressure difference p_Δ.
- The movement of the reed controls the volume flow through the reed channel and into the mouthpiece.

2.2 Vibrations of the Reed

- Some of the earliest research on musical instrument reeds was conducted by Helmholtz, who concluded that pipes excited by inwardly striking reeds "of light material which offers but little resistance" produce tones at frequencies corresponding to the resonant frequencies of the pipe, which are much lower than the natural frequency of the reed itself [Helmholtz, 1954, p. 390].
- The lowest resonance frequency of a typical clarinet reed falls approximately in the range 2-3 kHz, while normal playing frequencies for clarinets are below 1 kHz.

- A mass-spring system driven at a frequency well below resonance is said to be stiffness dominated and its displacement amplitude will approach f/k, where k is the spring constant and f is the applied force.
- Thus, a common simplification for woodwind instruments has been to neglect the effect of the mass altogether, which is equivalent to assuming an infinite reed resonance frequency, and to model the reed system as a memory-less system as depicted in Fig. 8 [Backus, 1963, Nederveen, 1969, McIntyre et al., 1983].

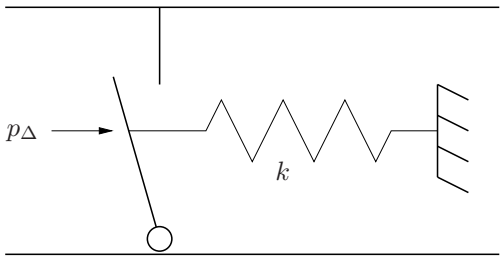

Figure 8: The single-reed as a mechanical spring blown closed.

- Observations by Backus [1961] of reed motion and mouthpiece pressure in an artificially blown clarinet appear to confirm that the reed is primarily stiffness controlled.
- Assuming the force on the reed is equal to $A_r \cdot p_\Delta$, where A_r is the effective surface area of the reed exposed to p_Δ, the reed tip opening with respect to its equilibrium position H is given by Hooke's law as

$$x = H - \frac{A_r \cdot p_\Delta}{k}. \tag{19}$$

- In this case, the motion of the reed is exactly "in-phase" with the pressure (p_Δ) acting on it.

2.3 Flow Through the Reed Orifice

- The flow through the reed orifice is typically determined using the Bernoulli equation for steady, laminar flow of an incompressible fluid [Backus, 1963, Worman, 1971, Wilson and Beavers, 1974, Thompson, 1979, Saneyoshi et al., 1987, Fletcher and Rossing, 1991].
- Relating pressure (p) and velocity (v) at any two points of height y within a continuous *tube of flow*, the Bernoulli equation is given by

$$p_1 + \frac{1}{2}\rho\, v_1^2 + \rho\, g\, y_1 = p_2 + \frac{1}{2}\rho\, v_2^2 + \rho\, g\, y_2, \tag{20}$$

  where ρ is fluid density and g is the acceleration of gravity. This expression is based on continuity of volume flow and conservation of energy.
- For the reed geometry as approximated in Fig. 9, the upstream cavity is viewed as a large tank of constant or slowly varying pressure p_u and essentially zero volume flow u_u.
- Application of the Bernoulli equation, assuming no appreciable change in height, leads to an expression for the flow through the reed orifice of the form

$$u = w\, x \left(\frac{2\,|p_\Delta|}{\rho}\right)^{1/2} \mathrm{sgn}(p_\Delta), \tag{21}$$

  where w and x are the width and height of the reed channel, respectively, and the sign function is

$$\mathrm{sgn}(p_\Delta) = \begin{cases} +1 & \text{if } p_\Delta \geq 0 \\ -1 & \text{otherwise.} \end{cases}$$

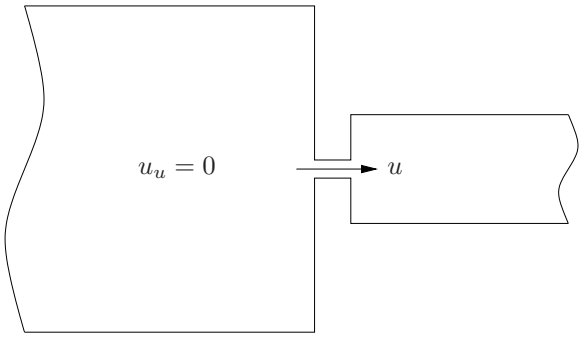

Figure 9: An approximate reed orifice geometry.

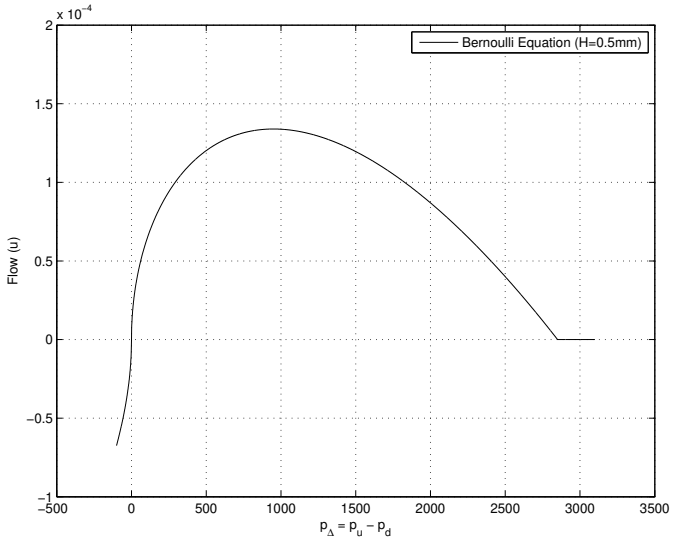

Figure 10: Flow characteristic through the reed orifice.

- An example flow curve determined using Eqs. (21) is shown in Fig. 10.
- Although the flow expression of Eq. (21) is derived for steady flow, its use is generally assumed to be valid under oscillating conditions as well (referred to as "quasi-static"). The validity of this assumption has been questioned by results of da Silva et al. [2007] and others.
- The acoustic resistance to flow presented by the orifice is inversely proportional to the slope of the flow curves in Fig. 10 [Fletcher and Rossing, 1991]. For low values of p_Δ, the resistance is given by a small positive value. At very high pressure differences, the reed is blown closed against the mouthpiece facing and all flow ceases.
- The threshold blowing pressure, which occurs at the flow peak, can be determined from Eqs. (21) and (19) and is roughly equal to 1/3 the closure pressure. Between the threshold and closure pressures, the flow resistance is negative and the reed mechanism functions as an acoustic generator.

2.4 The Reed-Spring Solution

- Under the previous assumption that the reed can be adequately modeled as a mechanical spring, the motion of which is in phase with the pressure (p_Δ) acting across it, Eq. (21) can be rewritten using

Eq. (19) as

$$\begin{aligned} u &= w\left(H - \frac{A_r \cdot p_\Delta}{k}\right)\left(\frac{2p_\Delta}{\rho}\right)^{1/2} \mathrm{sgn}(p_\Delta) \\ &= wH\left(1 - \frac{p_\Delta}{p_c}\right)\left(\frac{2p_\Delta}{\rho}\right)^{1/2} \mathrm{sgn}(p_\Delta), \end{aligned} \tag{22}$$

where $p_c = kH/A_r = \mu_r H \omega_r^2$ is the pressure necessary to push the reed against the mouthpiece facing and completely close the reed channel.

- The flow through the reed orifice is assumed to separate and form a free jet at the air column entrance. In the ensuing region of turbulence, the pressure is assumed equivalent to the reed channel pressure and conservation of volume flow to hold.
- In this case, $u = u_d$ and we can use Eq. (22) and the relation

$$u_d(t) = u_d^+(t) + u_d^-(t) = Z_c^{-1}[p_d^+(t) - p_d^-(t)], \tag{23}$$

to find a set of solutions for various values of p_Δ.

- The approach of McIntyre et al. [1983] is to assume a constant upstream pressure (p_u) and obtain solutions for the outgoing downstream pressure p_d^+ based on incoming pressures p_d^-. This amounts to finding the intersection of the flow curve and a straight line corresponding to Eq. (23), as illustrated in Fig. 11 below.

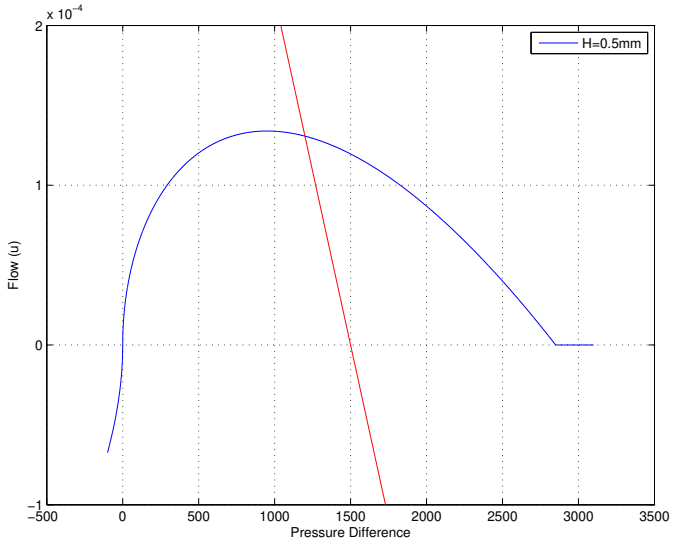

Figure 11: Flow and bore characteristic curves.

- However, it is preferable to maintain the dependence on p_Δ, which allows us to modify the mouth pressure in a time-domain simulation.
- Note that

$$\begin{aligned} p_d^+ - p_d^- &= p_d^+ - p_d^- + [p_u - p_u] + [p_d^- - p_d^-] \\ &= p_u - 2p_d^- - p_u + [p_d^+ + p_d^-] \\ &= p_\Delta^- - p_\Delta, \end{aligned} \tag{24}$$

where $p_\Delta^- = p_u - 2p_d^-$ consists of pressure components known or computable from previous values.

- We can then find a table of solutions, such as shown in Fig. 12, for the equation $Z_c\, u_d(p_\Delta) = p_\Delta^- - p_\Delta$.
- For values of p_Δ^- greater than p_c, the reed is closed and the solutions are given by a straight line of slope one, which corresponds to zero flow and pressure reflection without inversion at the junction.
- Thus, when the reed is forced against the mouthpiece facing, the air column appears as a rigidly terminated or stopped end.

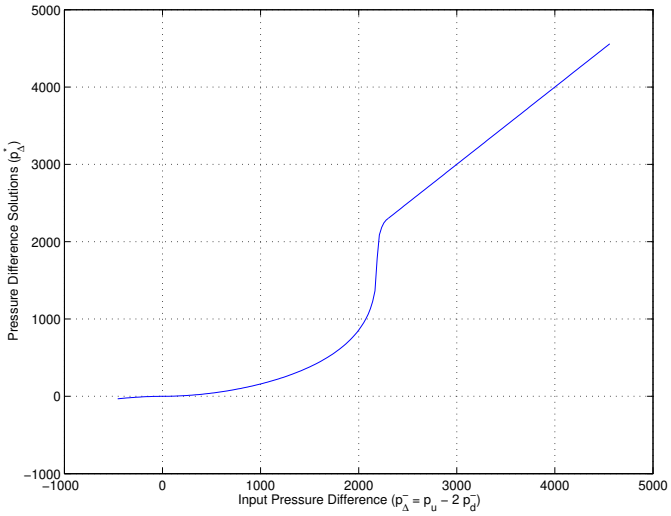

Figure 12: Solutions at reed/air column junction for input p_Δ^- ($p_c = 2280$ Pascals).

2.5 Reed Scattering Theory

- Alternately, the reed mechanism can be viewed as having a "lumped," pressure dependent impedance given by:

$$Z_r(p_\Delta) = \frac{p_\Delta}{u(p_\Delta)}. \tag{25}$$

- Under the assumption that the reed motion is adequately described as "stiffness dominated" and in-phase with the driving pressure and that the resulting volume flow through the reed slit is also frequency-independent (ignoring the inertance of the air in the reed channel), this characterization can be evaluated in the time domain as a memory-less non-linearity.
- Viewing the reed/air column junction using scattering theory as seen from the air column side, pressure-wave reflection from an impedance of Z_R is given by:

$$Z_r = \frac{P^+ + P^-}{(P^+ - P^-)/Z_c} \tag{26}$$

$$\frac{P^-}{P^+} = \frac{Z_r - Z_c}{Z_r + Z_c} = \frac{1 - Z_c/Z_r}{1 + Z_c/Z_r} \tag{27}$$

- The reed interface is then modeled with a nonlinear pressure-dependent reflection coefficient ($\rho(p_\Delta)$) given by Eq. (27) and implemented via a scattering junction as shown in Fig. 13. The pressure entering the downstream instrument air column is determined as [Smith, 1986]:

$$\begin{aligned} p_d^+ &= p_d^- \cdot \rho(p_\Delta) + p_u^+ \left[1 - \rho(p_\Delta)\right] \\ &= p_u^+ - \left[p_u^+ - p_d^-\right] \rho(p_\Delta). \end{aligned} \tag{28}$$

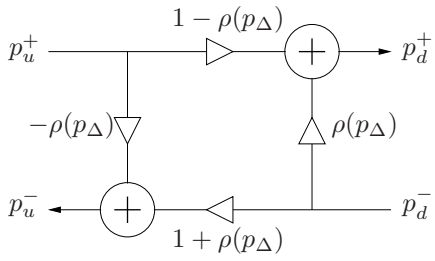

Figure 13: The reed scattering junction.

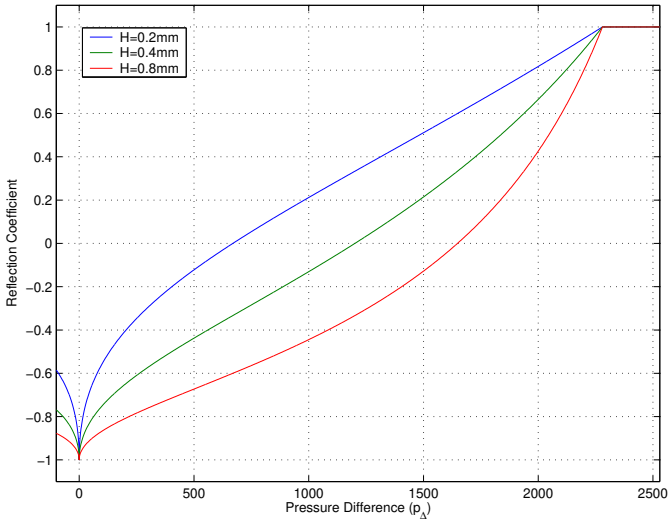

Figure 14: Reed/air column reflection coefficient values for different values of equilibrium tip opening (H).

- The reflection coefficient defined by the Bernoulli flow expression of Eq. (21) is shown in Fig. 14.
- For values of $p_\Delta > p_c$, the pressure reflection coefficient has unity gain. This corresponds to reflection from a rigidly stopped end, as mentioned previously.
- A coefficient value of zero corresponds to a junction without discontinuity.
- A coefficient of -1.0 corresponds to an ideally open-pipe end (a reed mechanism of zero impedance).
- For normal reed mechanisms with a narrow-slit geometry, it seems impossible that the reed/bore junction could ever be characterized by a reflection coefficient of zero or lower. It is expected that the impedance of the reed slit, even when unblown, has some minimum value (probably frequency-dependent, but we'll ignore that for now) greater than Z_c.

2.6 The Reed as a Mass-Spring-Damper System

- While the normal playing range of clarinets and saxophones is typically well below the first resonance frequency of the reed, extended range techniques are becoming an increasingly common part of contemporary performance practice.
- In reality, the reed has some non-zero mass (the effective mass may vary with displacement and lip position) so that some phase delay will occur as the vibrating frequency of the reed increases. This behavior could have an important affect on the response of the instrument.

- The most common approach is to model the reed as a simple damped mechanical oscillator, as depicted in Fig. 15, with an equation of motion of the form

$$m\frac{d^2x}{dt^2} + b\frac{dx}{dt} + kx(t) = A_r\, p_\Delta(t), \tag{29}$$

where m is the equivalent reed mass, k is the reed spring constant, and b is the damping factor.

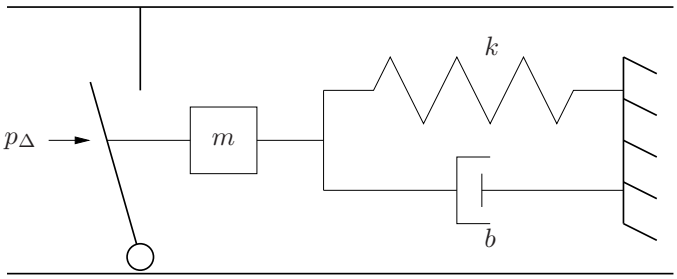

Figure 15: The single-reed as a mechanical oscillator blown closed.

- A substantial portion of the damping comes from the player's lower lip.
- Again, the reed motion is "displacement limited" by the mouthpiece facing.
- The natural frequency of the system in the absence of damping and for constant reed parameters is $\omega_r = \sqrt{k/m}$. Equation (29) is commonly expressed as

$$\ddot{x}(t) + g_r\dot{x}(t) + \omega_r^2 x(t) = \frac{p_\Delta(t)}{\mu_r}, \tag{30}$$

where g_r is the reed damping coefficient and μ_r is the reed's dynamic mass per unit area.

2.7 The Mass-Spring-Damper Solution

- As previously indicated, the flow through the reed channel is approximated "quasi-statically" using the Bernoulli equation and given by

$$u = w\,(x + H)\left(\frac{2\,|p_\Delta|}{\rho}\right)^{1/2}\mathrm{sgn}(p_\Delta), \tag{31}$$

where w is the reed channel width, x is the time-varying reed position, calculated from Eq. (29), and H is the equilibrium tip opening.

- For single-reed geometries, the pressure and flow in the reed channel can be approximated as equivalent to the pressure and flow at the entrance to the instrument air column. This approximation is based on continuity and detachment of volume flow at the end of the reed channel such that pressure is not recovered in the mouthpiece.
- Thus, the acoustic interaction at the interface of the reed and air column can be solved using Eqs. (29) and (31), together with a description of the input impedance of the attached air column.
- For a cylindrical pipe, we can compute the impedance using the digital waveguide structure of Fig. 16.
- From Fig. 16, it is clear that

$$p_0 = 2p_0^- + Z_c u_0, \tag{32}$$

where p_0^- is the traveling-wave pressure entering the reed junction from the downstream air column.

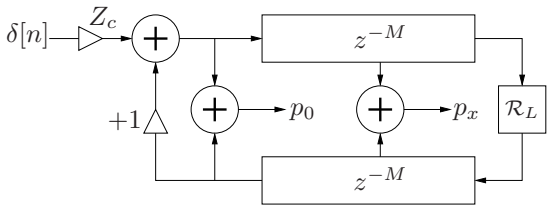

Figure 16: A digital waveguide cylindrical pipe impedance model (from Scavone [1997]).

- Because of mutual dependencies, however, an explicit solution of these equations can be problematic. In a discrete-time computational context, these mutual dependencies can be understood to result in delay-free loops.
- In Guillemain et al. [2005], the reed system is discretized using a centered finite difference approximation that avoids a direct feedforward path through the reed transfer function. The resulting system equations can then be expressed in terms of a second-order polynomial equation and an explicit solution found.
- The centered finite-difference approximation of Eq. (29) results in a digital filter structure of the form

$$\frac{X(z)}{P_\Delta(z)} = \frac{-z^{-1}/\mu_r}{(f_s^2 + \frac{g_r f_s}{2}) + (\omega_r^2 - 2f_s^2)z^{-1} + (f_s^2 - \frac{g_r f_s}{2})z^{-2}}, \tag{33}$$

  where f_s is the computational sample rate.
- As noted in Guillemain [2004], however, this filter structure is only stable for $\omega_r < f_s\sqrt{4 - (g_r/\omega_r)^2}$, limiting its use at low sample rates and/or with high reed resonance frequencies.
- A direct application of the bilinear transform to the system of Eq. (29) results in a digital filter structure given by

$$\frac{X(z)}{P_\Delta(z)} = \frac{-1/\mu_r \left[1 + 2z^{-1} + z^{-2}\right]}{a_0 + 2(\omega_r^2 - \alpha^2)z^{-1} + (\alpha^2 - g_r\alpha + \omega_r^2)z^{-2}}, \tag{34}$$

  where $a_0 = \alpha^2 + g_r\alpha + \omega_r^2$ and α is the bilinear transform constant that controls frequency warping.
- Note that we can achieve an exact continuous- to discrete-time frequency match at the resonance frequency of the reed by setting $\alpha = \omega_r / \tan(\omega_r/2f_s)$.
- In this case, the use of the bilinear transform guarantees a stable digital filter at any sample rate. The presence of the direct feedforward path in Eq. (34), however, prohibits the explicit reed interface solution mentioned above.
- We therefore seek an alternative form of Eq. (34) that preserves stability and avoids an undelayed feedforward coefficient in the transfer function numerator.
- By default, the bilinear transform substitution produces a system with "zeroes" at $z = \pm 1$ (or at frequencies of 0 and $f_s/2$ Hz). While this result is often desirable for digital resonators, we can modify the numerator terms without affecting the essential behavior and stability of the resonator.
- In fact, it is the numerator terms that control the phase offset of the decaying oscillation. Thus, we can modify and renormalize the numerator to produce a filter structure of the form

$$\frac{X(z)}{P_\Delta(z)} = \frac{-4z^{-1}/\mu_r}{a_0 + 2(\omega_r^2 - \alpha^2)z^{-1} + (\alpha^2 - g\alpha + \omega_r^2)z^{-2}}. \tag{35}$$

- The frequency- and time-domain responses of the centered finite-difference and "modified" bilinear transform filter structures are shown in Fig. 17 for a reed resonance frequency $f_r = 2500$ Hz and $f_s = 22050$ Hz.

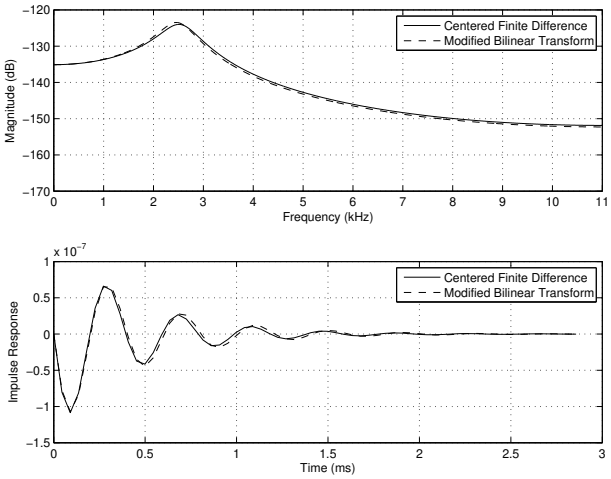

Figure 17: Reed filter frequency and impulse responses for centered finite-difference and modified bilinear transform structures with $f_r = 2500$ Hz and $f_s = 22050$ Hz: magnitude frequency response (top) and impulse response (bottom).

- The complete clarinet model involves the calculation of the reed displacement using this stable reed model, the volume flow through the reed channel as given by Eq. (31), and the relationship between flow and pressure at the entrance to the air column as given by Eq. (32).
- Because the reed displacement given by Eq. (35) does not have an immediate dependence on p_Δ, it is possible to explicitly solve Eqs. (32) and (21), as noted in Guillemain et al. [2005], by an expression of the form

$$u_0 = 0.5 \left(B\sqrt{(Z_c B)^2 + 4A} - Z_c B^2 \right) \mathrm{sgn}(A), \tag{36}$$

  where $A = p_m - 2p_0^-$ and $B = w\,(x + H)(2/\rho)^{1/2}$ can be determined at the beginning of each iteration from constant and past known values.
- Whenever the reed channel height $x + H < 0$, u_0 is set to zero and $p_0 = 2p_0^-$.
- In Fig. 18, the normalized pressure response of the complete DW synthesis model is plotted using both reed models with $f_r = 2500$ Hz and $f_s = 22050$ Hz.
- The behaviors are indistinguishable for these system parameters, though as indicated above it is possible to run the modified bilinear transform model at significantly lower sample rates (and with higher reed resonance frequencies).

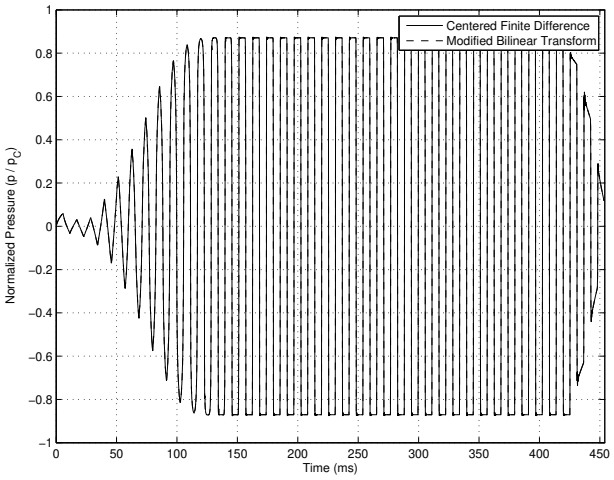

Figure 18: Normalized pressure response from complete DW synthesis model using the centered finite-difference and modified bilinear transform structures with $f_r = 2500$ Hz and $f_s = 22050$ Hz.

2.8 Refinements

Much of the discussion thus far has been based on rather ideal behaviors and/or system properties. Despite that, these analyses provide good "first-order" descriptions for the various components of the reed mechanism and together, capture the fundamental response of the overall system. Below, we discuss a number of incremental refinements that have been proposed to these equations.

- The motion of the reed is expected to induce a flow contribution of its own proportional to $A_r\dot{x}(t)$.
- The flow that enters the reed channel from the upstream side is therefore considered to divide into a component u_d entering the downstream air column and the volume flow swept out by the reed,

$$u(t) = u_d(t) + A_r\dot{x}(t). \tag{37}$$

- This extra flow component has been shown to have some significant influence on playing frequencies as predicted from analytical and numerical simulations [Coyle et al., 2015].
- Stewart and Strong [1980] and Sommerfeldt and Strong [1988] modeled the reed as a damped, driven, nonuniform bar using a fourth-order differential equation. In this way, changes in effective mass and stiffness with bending along the curvature of the lay are automatically incorporated.
- Avanzini and van Walstijn [2004] also modeled the reed as a clamped-free bar using finite difference techniques and derived appropriate parameters from measurements and tuning. These results were then used to develop a non-linear lumped model [van Walstijn and Avanzini, 2007].
- More recent models of reed stiffness include an extra force term which only becomes active when the reed displacement goes beyond a certain distance, thus effectively producing a non-linear spring effect [Chatziioannou and van Walstijn, 2012].
- An additional force on the reed caused by higher localized volume flow within the reed channel was proposed by Worman [1971] and had been included in a few later reed analyses [Benade, 1976, Schumacher, 1981, Keefe, 1990b]. For such a force to exist, the reed channel height must be non-uniform or the flow must separate at the channel entrance and then subsequently reattach at a further point in the channel. Hirschberg et al. [1990] point out that there are incompatibilities in the derivation of the "Bernoulli" force that make its application to the clarinet reed mechanism questionable.

2.9 The Brass Lip Mechanism

- The brass lip mechanism functions as a pressure-controlled valve that admits a puff of air whenever the pressure is high in the mouthpiece.
- Because the resonance frequency of the brass lip mechanism must nearly match the desired sounding frequency of the instrument (hopefully with support from an air column resonance at or near that frequency), the mass component of the lips cannot be ignored.

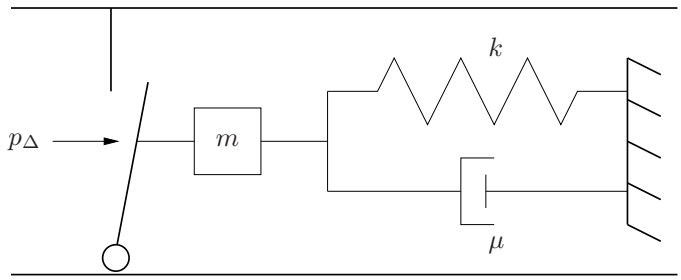

Figure 19: The brass player's lips as a mechanical oscillator blown open.

- Pressure pulses reflected back from the far end of the horn tend to force the player's lips open ... positive feedback.
- While one might expect the lips to be blown closed when the mouthpiece pressure is high, it should be remembered that the mass in a mass-spring-damper system lags behind the driving force by 1/4 cycle at its resonance frequency (as shown in Fig. 20). During this "lag time", the lip valve is open and flow through the valve can augment the positive mouthpiece pressure.

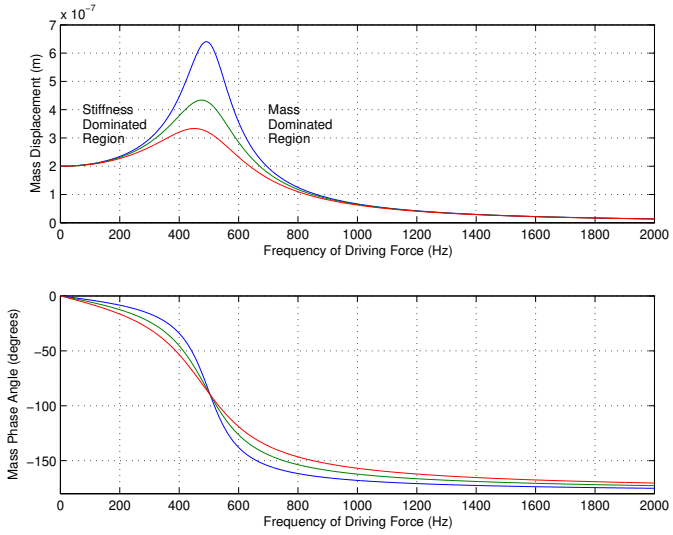

Figure 20: Displacement and phase of a mass-spring-damper system.

- The player controls the resonance frequency of his/her lips via tension and mass (position) variations.
- Oscillations are favored when the air column has one or more resonances that correspond to the harmonics of the fundamental pitch.

- Most of the equations discussed earlier for the woodwind reed valve can also be applied to the brass lip mechanism. The primary distinction concerns the equations of lip displacement. The lips are initially closed but then blown open.
- Attempts to model the lip mechanism have included both "swinging-door" and "up-down" displacement trajectories.

References

F. Avanzini and M. van Walstijn. Modelling the mechanical response of the reed-mouthpiece-lip system of a clarinet. Part 1. A one-dimensional distributed model. *Acta Acustica united with Acustica*, 90(3):537–547, 2004.

J. Backus. Vibrations of the reed and air column in the clarinet. *Journal of the Acoustical Society of America*, 33(6):806–809, Mar. 1961.

J. Backus. Small-vibration theory of the clarinet. *Journal of the Acoustical Society of America*, 35(3): 305–313, Mar. 1963.

A. H. Benade. *Fundamentals of Musical Acoustics*. Oxford University Press, New York, 1976.

V. Chatziioannou and M. van Walstijn. Estimation of clarinet reed parameters by inverse modeling. *Acta Acustica united with Acustica*, 98:628–639, 2012.

W. Coyle, P. Guillemain, J. Kergomard, and J. Dalmont. Predicting playing frequencies for clarinets: A comparison between numerical simulations and simplified analytical formulas. *Journal of the Acoustical Society of America*, 138(5):2770–2781, 2015.

A. da Silva, G. Scavone, and M. van Walstijn. Numerical simulations of fluid-structure interactions in single-reed mouthpieces. *Journal of the Acoustical Society of America*, 122(3):1798–1810, 2007.

J. Dalmont, C. J. Nederveen, V. Dubos, S. Ollivier, V. Méserette, and E. Sligte. Experimental determination of the equivalent circuit of an open side hole: Linear and non linear behavior. *Acta Acustica*, 88:567–575, 2002.

V. Dubos, J. Kergomard, A. Khettabi, J. Dalmont, D. Keefe, and C. Nederveen. Theory of sound propagation in a duct with a branched tube using modal decomposition. *Acta Acustica*, 85:153–169, 1999.

N. H. Fletcher and T. D. Rossing. *The Physics of Musical Instruments*. Springer-Verlag, New York, 1991.

P. Guillemain. A digital synthesis model of double-reed wind instruments. *Eurasip Journal on Applied Signal Processing*, 4(7):990–1000, June 2004.

P. Guillemain, J. Kergomard, and T. Voinier. Real-time synthesis of clarinet-like instruments using digital impedance models. *Journal of the Acoustical Society of America*, 118(1):483–494, July 2005.

H. Helmholtz. *On the Sensations of Tone as a Physiological Basis for the Theory of Music*. Dover Publications, Inc., New York, 1954. Translated by Alexander J. Ellis from the 4th German Edition of 1877.

A. Hirschberg, R. W. A. van de Laar, J. P. Marrou-Maurières, A. P. J. Wijnands, H. J. Dane, S. G. Kruijswijk, and A. J. M. Houtsma. A quasi-stationary model of air flow in the reed channel of single-reed woodwind instruments. *Acustica*, 70(2):146–154, Feb. 1990.

D. H. Keefe. *Woodwind Tone-hole Acoustics and the Spectrum Transformation Function*. PhD thesis, Case Western Reserve University, 1981.

D. H. Keefe. Woodwind air column models. *Journal of the Acoustical Society of America*, 88(1):35–51, July 1990a.

D. H. Keefe. On sound production in reed-driven wind instruments. Technical report, University of Washington, School of Music, Systematic Musicology Program, Seattle, Washington, Report No. 9003, 1990b.

J. L. Kelly, Jr. and C. C. Lochbaum. Speech synthesis. In *Proceedings of the Fourth International Congress on Acoustics*, pages 1–4, Copenhagen, Denmark, Sept. 1962. Paper G42.

A. Lefebvre and G. P. Scavone. Characterization of woodwind instrument toneholes with the finite element method. *Journal of the Acoustical Society of America*, 131(4):3153–3163, 2012.

M. E. McIntyre, R. T. Schumacher, and J. Woodhouse. On the oscillations of musical instruments. *Journal of the Acoustical Society of America*, 74(5):1325–1345, nov 1983.

C. J. Nederveen. *Acoustical Aspects of Woodwind Instruments*. Frits Knuf, Amsterdam, The Netherlands, 1969.

C. J. Nederveen, J. Jansen, and R. van Hassel. Corrections for woodwind tonehole calculations. *Acta Acustica*, 84:957–966, 1998.

A. V. Oppenheim and R. W. Schafer. *Discrete-Time Signal Processing*. Prentice Hall, Inc., Englewood Cliffs, New Jersey, 1989.

J. Saneyoshi, H. Teramura, and S. Yoshikawa. Feedback oscillations in reed woodwind and brasswind instruments. *Acustica*, 62:194–210, 1987.

G. P. Scavone. *An Acoustic Analysis of Single-Reed Woodwind Instruments with an Emphasis on Design and Performance Issues and Digital Waveguide Modeling Techniques*. PhD thesis, Music Dept., Stanford University, March 1997.

R. T. Schumacher. *Ab Initio* calculations of the oscillations of a clarinet. *Acustica*, 48(2):71–85, 1981.

J. O. Smith. Efficient simulation of the reed-bore and bow-string mechanisms. In *Proceedings of the 1986 International Computer Music Conference*, pages 275–280, The Hague, Netherlands, 1986. Computer Music Association.

S. D. Sommerfeldt and W. J. Strong. Simulation of a player-clarinet system. *Journal of the Acoustical Society of America*, 83(5):1908–1918, May 1988.

S. E. Stewart and W. J. Strong. Functional model of a simplified clarinet. *Journal of the Acoustical Society of America*, 68(1):109–120, July 1980.

S. C. Thompson. The effect of the reed resonance on woodwind tone production. *Journal of the Acoustical Society of America*, 66(5):1299–1307, Nov. 1979.

V. Välimäki, M. Karjalainen, and T. I. Laakso. Modeling of woodwind bores with finger holes. In *Proceedings of the 1993 International Computer Music Conference*, pages 32–39, Tokyo, Japan, 1993. Computer Music Association.

M. van Walstijn and F. Avanzini. Modelling the mechanical response of the reed-mouthpiece-lip system of a clarinet. Part 2. A lumped model approximation. *Acta Acustica united with Acustica*, 93:435–446, 2007.

T. A. Wilson and G. S. Beavers. Operating modes of the clarinet. *Journal of the Acoustical Society of America*, 56(2):653–658, Aug. 1974.

W. E. Worman. *Self-Sustained Nonlinear Oscillations of Medium Amplitude in Clarinet-Like Systems*. PhD thesis, Case Western Reserve University, 1971.